

Quantitative video-rate hydration imaging of Nafion proton exchange membranes with terahertz radiation

D. F. Alves-Lima, R. Letizia, R. Degl'Innocenti, R. Dawson, H. Lin*

Department of Engineering, Lancaster University, Lancaster, LA1 4YR, United Kingdom

* h.lin2@lancaster.ac.uk

+44 (0)1524 593013

D19 D – Floor

Engineering Building

Lancaster University

Bailrigg, Lancaster

United Kingdom

LA1 4YR

Abstract

Nafion membranes are considered as the industry standard electrolyte material for proton exchange membrane fuel cells. These membranes require adequate hydration in order to reach a high proton conductivity. The relatively high sensitivity of terahertz radiation to liquid water enables contrast to be observed for inspecting water presence in Nafion electrolyte membranes. Utilising a commercially available terahertz source and camera, this paper investigates the feasibility of a compact terahertz imaging system for visualising and quantifying liquid water during an ambient air desorption process for Nafion membranes of a wide range of thicknesses – NRE-212 (50 μm), N-115 (127 μm), N-117 (180 μm) and N-1110 (254 μm). We demonstrate that the terahertz imaging system is able to quantify liquid water in the 25-500 μm thickness range, estimate membrane weight change related to liquid water desorption, which correlated well against simultaneous gravimetric analysis and visualise the room temperature liquid water desorption process of a partially hydrated Nafion N-117 membrane.

Keywords:

Terahertz imaging; Nafion; hydration; fuel cell;

1. Introduction

Polymer electrolyte membrane fuel cells (PEMFC) are electrochemical devices at the forefront of clean energy production for portable, transportation and, to a lesser extent, stationary applications [1]. During the fuel cell operation, protons emerging from the anodic hydrogen oxidation flow across the polymer electrolyte membrane (PEM) to the cathode, and combine with electrons and oxygen to form water. The most common material for PEM is a perfluorinated ionomer copolymer known as Nafion, consisting in perfluorovinyl ether groups terminated with sulfonate groups incorporated onto a tetrafluoroethylene (PTFE) backbone [2]. Liquid water uptake is known to enhance proton conduction in Nafion [3–5]. In addition, homogeneous hydration aids in maintaining uniform membrane impedance, where protonic current is similar across all the PEM area. Failure to achieve this will result in protonic current gradients, localised hotspots (as internal resistance increases) and pinhole formation, possibly resulting in PEMFC failure [6]. Achieving uniform PEM hydration during operation is a challenge, as regions across the membrane near the inlets tend to be drier due to an increased reactant gas pressure, but become increasingly humid near the outlets as a result of downstream water transport with the reactant gas. Water thus plays an interesting role in PEMFC operation: Nafion PEM requires hydration to operate and hence reactant inlet streams are humidified [7],

but at the same time, water is a by-product of the electrochemical half-reaction at the cathode and therefore must be swiftly removed to prevent cell flooding and reactant starvation at active electrocatalyst sites [8]. For water fault diagnosis, various methods exist such as the assessment of pressure drop [9], electrochemical impedance spectroscopy (EIS) [10], residence time distribution [11, 12]. However, one of the main drawbacks of these techniques is that they provide an indirect assessment of the entire operating fuel cell and do not allow one to localise the faults directly. Critical insights into the complex physical phenomena involving liquid water condensation and transport within the PEMFC can also be provided by imaging techniques, such as magnetic resonance imaging (MRI) [13–17], neutron [18–23], x-ray [24–29], infrared [30, 31], direct visualisation [32–37] and fluorescence microscopy [38, 39]. Extensive overview on the subject matter has been published elsewhere [40–43] but generally, MRI, neutron and x-ray imaging/tomography techniques can image through visually opaque components, such as the gas diffusion layers (GDL) and gas flow channels (GFC) [44], thus providing in-situ information on liquid water transport. However, main restrictions to these techniques are underpinned by equipment availability and temporal resolution, with the example of MRI requiring 50 s to acquire an image. Direct optical visualisation and infrared imaging can visualise liquid water through specially designed transparent PEMFCs and provide information on two-phase flow regimes in the GFC [35] at a relatively high temporal and spatial resolutions (30 Hz and 5 μm , respectively). Furthermore, when coupled with fluorescence microscopy, direct visualisation can illustrate ex-situ liquid water preferential transport patterns in the GDL [38, 39]. However, a key drawback is the opacity of common PEMFC components in the visible and infrared portion of the spectrum. Particularly in the context of off-line water uptake and retention studies in Nafion membranes, techniques such as dynamic vapour sorption, differential scanning calorimetry, EIS and confocal micro-Raman spectroscopy [45–51] have been used. Although these are sensitive measurements for water content in Nafion membranes, with μm resolution in the case of Raman spectroscopy, generally they cannot spatially resolve liquid water distribution over large areas at video-rate and may additionally require detailed sample preparation, calibration models, or specialised equipment with temperature and humidity control.

Terahertz (THz) radiation is situated on the electromagnetic spectrum between 100 GHz to 30 THz and can penetrate through dielectric materials, such as polymers, but is strongly absorbed by polar materials, such as liquid water. This in turn motivates the use of terahertz sensing for many non-destructive industrial applications such as in pharmaceutical film coatings monitoring [52–55], food contaminants detection [56] and defects identification [57]. Terahertz

sensing have also been actively applied in fuel cells, for example, Thamboon and Buaphad et al [58,59] employed narrowband terahertz reflection imaging to visualise liquid water in flow cell channels. Ray et al examined water retention on UV-treated sulfonated polyether ether ketone functionalised carbon nanotubes PEMs using terahertz time domain spectroscopy (THz-TDS) [60]. Devi et al, also using THz-TDS, monitored water retention in a hydrated Nafion membrane [61]. Measurements so far have demonstrated the sensitivity of terahertz radiation to monitor hydration in membranes. However, given that raster scanning is necessary to image water spatial distribution, which can take up to several minutes pending on integration time and scanned area, it will not be able to portray an accurate real-time water spatial distribution during a desorption process. Here we investigate the feasibility of a compact, portable, and video-rate 100 GHz imaging system for direct water visualisation and quantification in hydrated Nafion PEMs, as an initial route towards liquid water inspection in fully operating PEMFC. In particular, we validate the terahertz system's sensitivity for water quantification against known water thickness, and then estimate water weight in a wide range of Nafion membranes (50-254 μm thickness) across time, benchmarked against gravimetric analysis. Finally, to assess the system's ability to spatially resolve water distribution across a Nafion membrane, we imaged the desorption profile of a partially hydrated Nafion membrane at room temperature under ambient conditions.

2. Materials and Methods

2.1. Terahertz imaging system

The transmission terahertz imaging system uses an IMPATT diode source, operating at 100 GHz and at 100 mW output power, and a 16x16 terahertz camera with 1.5 mm pixel size and sensitivity in the 50-700 GHz frequency range (Terasense Inc., CA, USA). A polymethylpentene (TPX) plano-convex lens (Thorlabs, Inc.) is used to collimate the diverging terahertz beam, shown in Fig. 1. A custom-made liquid cell, which can confine water to a predefined thickness, is used to assess the system's ability to quantify liquid water. The cell is made out of stainless steel compressor plates with rectangular apertures fitted with terahertz transparent acrylic [62] windows and spacers, of thicknesses between 6 to 500 μm (Specac Ltd., Kent, UK; Davis Industrial Plastics, West Sussex, UK).

2.2. Gravimetric analysis

In order to validate the terahertz measurements, Nafion samples' weight loss was monitored during the water desorption process (Figure 1a). The weight balance used (Kern PCB 350-3)

had mg resolution at a 4 Hz data acquisition rate. Table 1 lists the Nafion membranes of varying complexity and thickness used in these studies:

Table 1 – Summary of the Nafion membranes used in the study.

Commercial name	Manufacturing process	Thickness (μm)	Supplier
NRE-212	Dispersion cast	50	Alfa Aesar (Lancashire, UK)
N-115	Extruded film	127	Fuel Cell Store (TX, USA)
N-117	Extruded film	180	Alfa Aesar (Lancashire, UK)
N-1110	Extruded film	254	Fuel Cell Store (TX, USA)

The membranes were measured as received, without further treatment. The dry membranes were cut into square patches ($\sim 70 \times 70 \text{ mm}^2$) and their weight and terahertz intensity images were acquired after drying for 1 hour in a laboratory oven (Carbolite ELF 11/14) at 105°C . The dry membranes were then equilibrated with deionised water at 80°C in order to enhance water uptake [63], where excess surface water was removed with paper wipes [64]. The hydrated sample, was then held in place to a sample holder with binder clips (Figure 1b) in order to dehydrate at room temperature. For each of the studied membranes, 4 repeats were performed. The water weight (W_{H_2O}) is calculated using Eq. (1):

$$W_{H_2O} = W(t) - W_{dry} \quad (1)$$

where $W(t)$ is the sample weight at a given time t and W_{dry} is the dry sample weight.

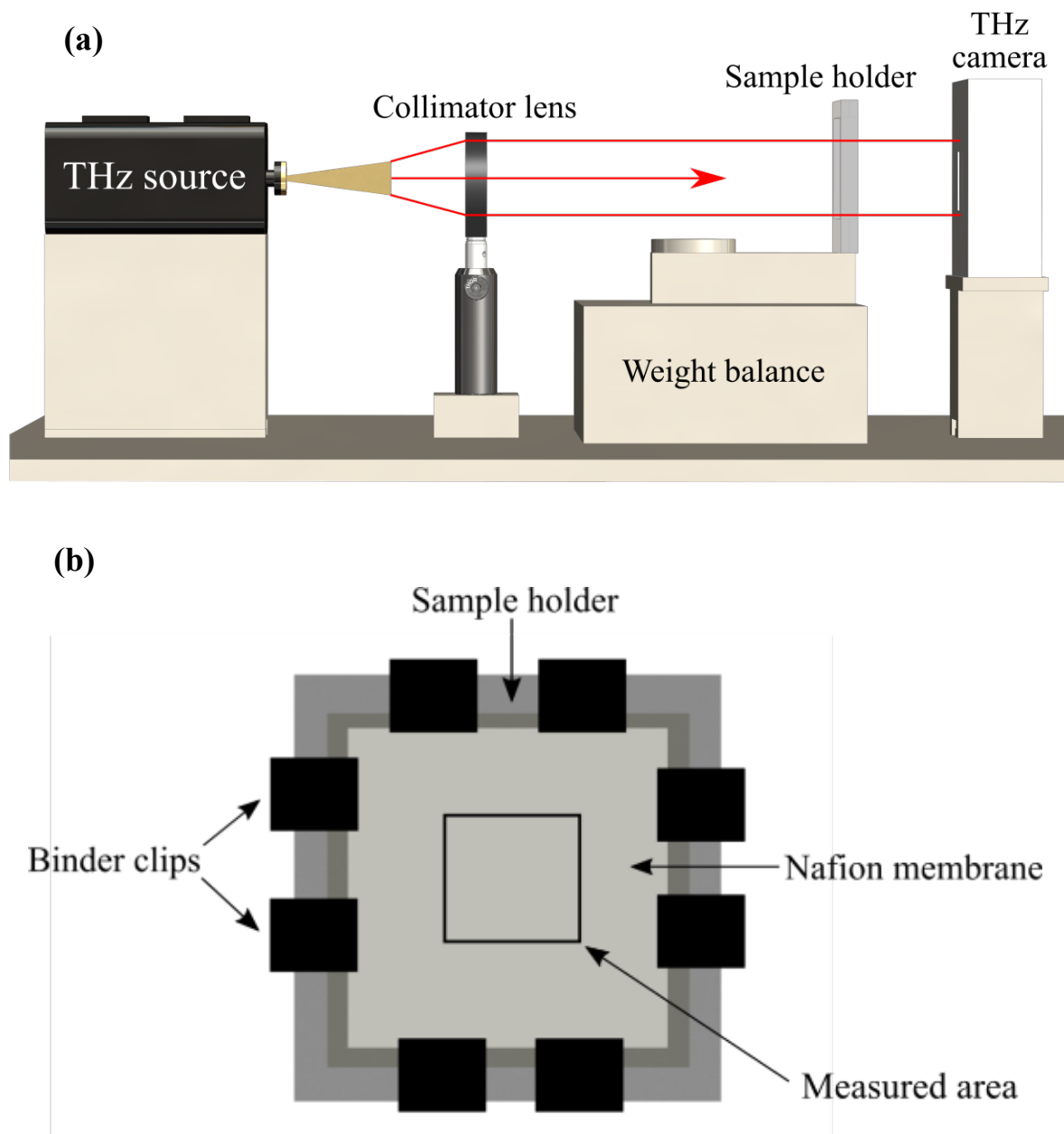


Figure 1 – (a) Schematic of the terahertz imaging system for simultaneous gravimetric analysis (b) Front view of the sample holder featuring Nafion sample, binder clips, and area used for terahertz measurements.

2.3. Data processing

The acquired terahertz intensity images were analysed using Matlab (Mathworks, Inc., MA, USA), and the code used for conversion is available in the supplementary information. The extracted frames are represented in false colours, with individual pixels representing light intensities between values of 0 (total absence of light, black) and 1 (total presence of light, white). Beer-Lambert Law relates light attenuation to material properties according to Eq. (2):

$$I/I_0 = \exp^{-\alpha d} \quad (2)$$

where I_o and I are the reference and sample light intensities, respectively, d is sample thickness and α is the material absorption coefficient (mm^{-1}) – taking on a value of 11 mm^{-1} as the average between $9\text{--}13 \text{ mm}^{-1}$ at 25°C at 100 GHz [65–69] for liquid water, and used for calculation purposes in this paper. Using Beer-Lambert law, water thickness in the area corresponding to a single pixel (d_{pixel}) can be estimated. The measured intensity from the dried membrane is used as the reference measurement in order to remove the effect of the Nafion membrane, thus isolating the response of absorbed liquid water. The estimated water thickness in each pixel (d_{pixel}), can be used to estimate water weight in each pixel, EW_{pixel} :

$$EW_{pixel} = A_{pixel}d_{pixel}\rho \quad (3)$$

where A_{pixel} and ρ correspond to pixel area and water density of at 1 g/cm^3 at 25°C , respectively. Equation (4) gives the estimated water weight (EW) in the entire membrane area:

$$EW = \frac{A_{membrane}}{A_{camera}} \sum_{pixel=1}^{196} EW_{pixel} \quad (4)$$

In order to avoid edge effects of the membrane and beam interference from the binder clips used to clamp the sample, we measured a small ($24 \times 24 \text{ mm}^2$) central portion of the sample (A_{camera}), shown in Figure 1b, whose edges are 18 mm away from the binder clips. The outermost rows and columns of pixels were discarded for liquid water weight estimation across the Nafion membranes due to random fluctuations observed in free space measurements. Therefore only the 14×14 remaining pixel matrix (196 pixels) was used. However, these discarded pixels are shown in Figures 2 and 5 to provide visual evidence of the camera's fluctuating edge effects but were not used in the respective analysis. In addition, the first term on Equation (4) extrapolates these results to the entire membrane area ($A_{membrane}$), assuming uniform water content distribution across a vertically mounted sample.

3. Results and discussion

3.1. Terahertz liquid water quantification

In order to assess the ability of the proposed terahertz imaging system to estimate liquid water thickness in the membrane, terahertz intensity images of the ‘dry’ and ‘hydrated’ liquid cell for a range of spacer thicknesses were acquired and compared. Figure 2 shows the intensity images for the $50 \text{ }\mu\text{m}$ spacer where there is a clear difference between the two images in the highlighted region of interest, approximately corresponding to the liquid cell's aperture. As expected in the presence of liquid water, intensity of terahertz transmission is notably reduced due to water absorption thus leading to lower detected values resulting in visibly ‘dimmer’ values on the

image in Fig. 2b. For quantification purposes, pixel values in the 3x4 pixels region of interest at the centre of the high transmission zone in dry (Fig. 2a) and hydrated states (Fig. 2b) are selected and compared.

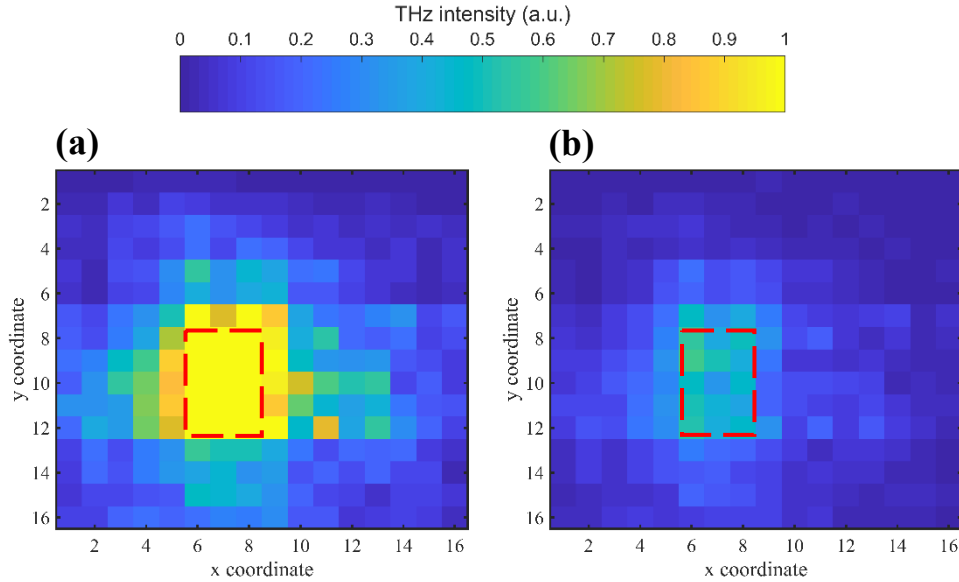


Figure 2–Terahertz false colour images of the (a) ‘dry’ and (b) ‘hydrated’ liquid cell of spacer thickness 50 μm . Highlighted region corresponds to the aperture in the liquid cell and is used for quantification purposes.

The relative transmitted intensity in each pixel (I) in the region of interest is given by Equation (6):

$$I = \frac{I_{hydrated}}{I_{dry}} \quad (6)$$

for different water thicknesses of 6, 12, 25, 50, 100, 200, 250 and 500 μm , as shown in Figure 3. This is plotted against the expected values from the Beer-Lambert law with variations in absorption coefficient. For the sake of clarity, the experimental relative transmitted intensity is calculated on a pixel-by-pixel basis, rather than pixel value averaging across the region of interest. The mean and standard deviation of the relative intensity of the region of interest pixels are then displayed as error bars in Figure 3. In addition, for each of the measured thicknesses, 5 repeats were taken.

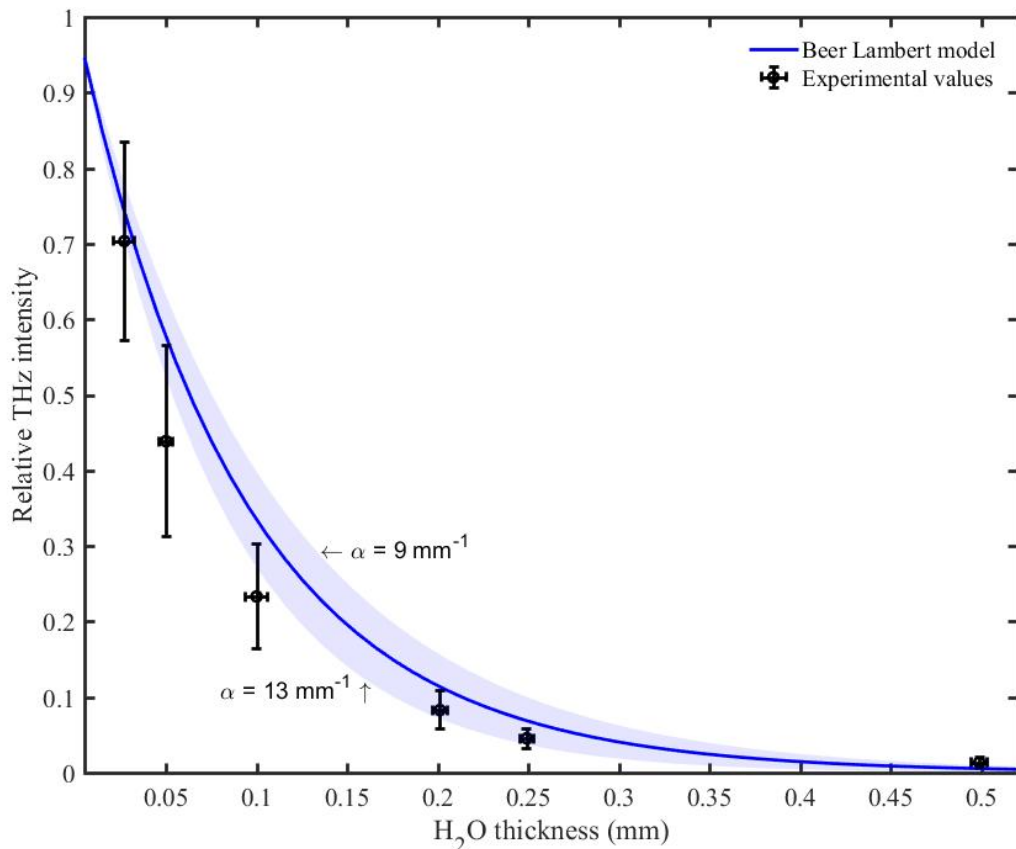


Figure 3 – Water quantitative analysis showing the measured relative transmitted terahertz intensities at a 25-500 μm range of liquid water thicknesses, against the expected values using Beer Lambert Law with absorption coefficients of 9-13 mm^{-1} at 100 GHz at 25°C, with maximum (13 mm^{-1}) and minimum (9 mm^{-1}) values displayed at the boundaries of shaded area. The vertical error bars refer to standard deviation between 5 experiments. The horizontal error bars refer to thickness tolerances of the spacer material.

It should be noted that, there were no discernible differences in pixel values between ‘dry’ and ‘hydrated’ terahertz intensity images for 6 and 12 μm spacer thicknesses due to the limited terahertz camera detection sensitivity, and thus these values are not shown in Figure 3. However, for increasing water thicknesses, there is an agreement against the expected values where terahertz transmission decays exponentially with increasing water. It is important to highlight that for 25 and 50 μm water thicknesses, there is a higher standard deviation between measurements when compared against 200 and 250 μm . This can be possibly due to decreasing systems detection sensitivity with decreasing water content. In addition, although 500 μm water thickness presents relatively low standard deviation (< 0.01 relative THz intensity), a water layer 500 μm -thick should theoretically attenuate over 99.5% of the incident terahertz beam and thus measurements in this region will have considerable uncertainty. Nevertheless, the data shows the system is able to quantify liquid water content, in the 25-500 μm detection range of water thicknesses, with a 25 μm limit of detection and 25 μm minimum sensitivity, given by

the smallest difference between calibration points (25 and 50 μm). Considering Schmidt-Rohr and Chen [70], we can assume that overall water thickness in the Nafion structure is comparable to the thickness of the membrane itself, and thus suggesting we can also quantify liquid water in Nafion membranes.

3.2. Liquid water weight estimation in Nafion membranes

Following on water thickness estimation in a liquid cell, we apply the thickness range estimated from relative intensity measurements from 3.1 to estimate the mass change, during a water desorption test in ambient air, for four different types of Nafion membranes benchmarked against simultaneous gravimetric analysis (Figure 4). This in turn allows us, to show the ability of a simple terahertz imaging system to quantify water across Nafion membranes. It should be noted that four repeats were performed for each of the membranes. Measured and estimated weights correspond to the weight change of water determined by simultaneous gravimetric analysis and terahertz intensity images, respectively.

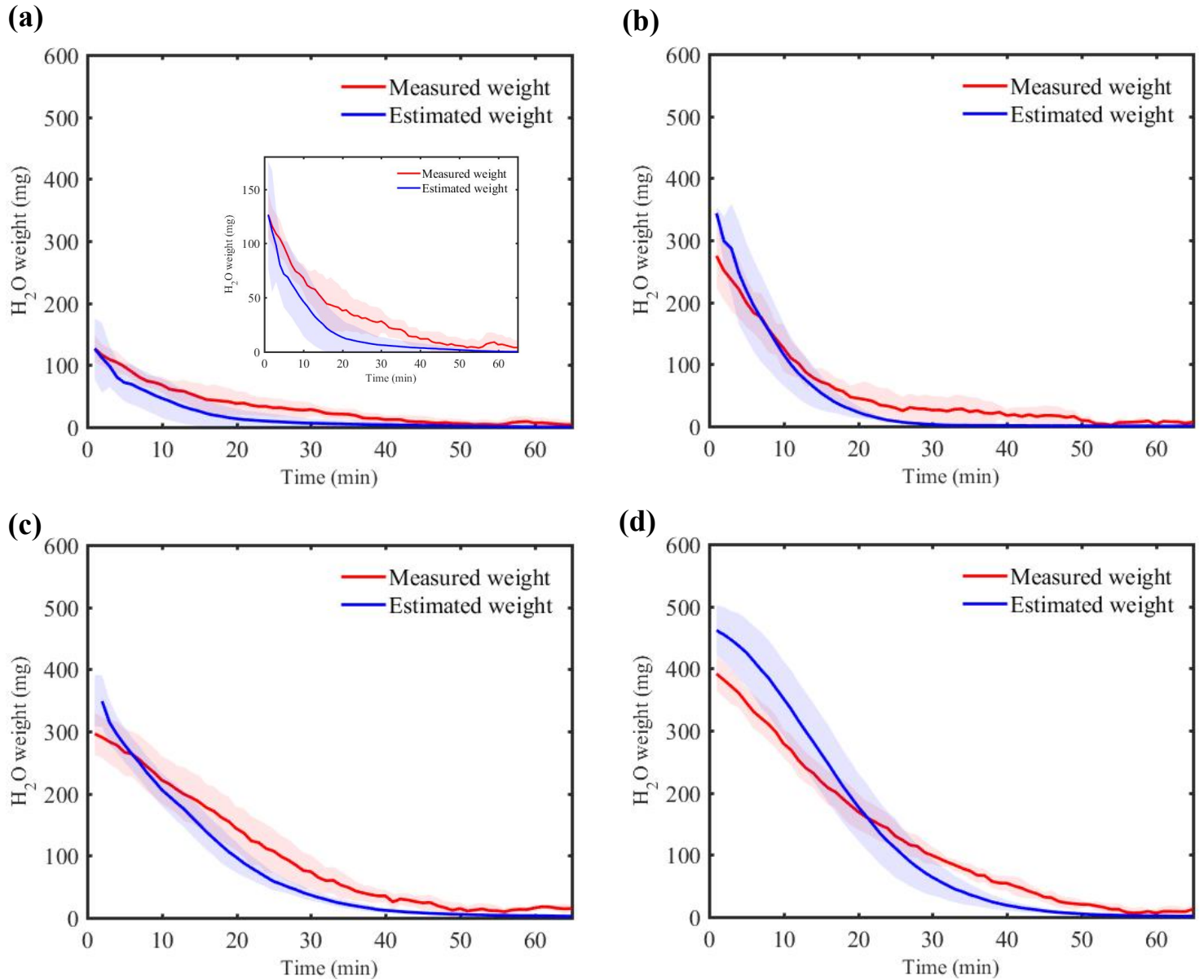


Figure 4 – Water desorption from saturated Nafion (a) NRE-212, (b) N-115, (c) N-117 and (d) N-1110. Blue and red line and shade represent the mean and standard deviation of estimated liquid water weight from terahertz intensities and actual measured liquid water weight from gravimetric analysis, respectively, from 4 repeated experiments. For clarity, a reduced scale inset is present on (a).

Fig. 4 shows a good agreement between the measurement and estimation curves, which shows an exponential decay consistent with prior water desorption studies in Nafion membranes [47,48,71,72]. However, there are notable differences between the curves, which can be consistently observed across the membranes. Firstly, the terahertz estimated weight overshoots the measured weight values. This can be attributed to the presence of residual liquid surface water that may be present in thicknesses outside the thickness range (25 – 500 μm) and the non-uniform water distribution across the membrane especially for a vertical sample mounting arrangement thus leading to higher estimated weight values. Secondly, differences are observed

between the time constants. It can be noted that after the initial minutes, the curves overlap with discrepancies appearing close to the end of measurement. This effect is predominantly shown in Figure 4a, from around 15-20 minutes until the 40 minute mark. The divergence in time constants between the curves is due to significant surface water accumulation under the binder clips, outside of the measurement area of the terahertz camera. Water loss in Nafion is usually attributed to diffusion from the interior of the membrane to the membrane/gas interface and subsequent transport into the gas phase, the latter being considered the key mechanism to this desorption process [71]. The region under the binder clips used as part of the experimental setup also has limited membrane/gas interface, so water loss happens at a slower rate because it is governed by an internal diffusion process only. Furthermore, as shown in section 2.2., our terahertz imaging system measures liquid water in the Nafion structure across a small area corresponding to the terahertz camera aperture while the gravimetric setup is measuring the weight of the entire sample holder structure, and therefore it is likely that this accumulated water is responsible for the increase in time constant of the measured weight curve.

The NRE-212 membrane presents clearly a higher level of standard deviation across repeats when compared to other membranes. This can be due to the presence of significant surface water in this membrane, which was challenging to remove thoroughly and consistently, as illustrated by the relatively large standard deviation in the terahertz measurement at the beginning of the experiment. The smaller thickness of Nafion NRE-212 at 50 μm also coincides with the system's reduced sensitivity at lower water thickness ranges as opposed to 100, 200 or 250 μm thus explaining why estimated weight values in Figure 4a present the highest variation.

By examining the water uptake of the individual membranes, shown by the initial water measured weight values, it also increases as the membrane thickness increases, consistent with Schmidt-Rohr and Chen [70]. However, the increase is not proportional to thickness, for example there is a large difference in water uptake between 50 μm thick NRE-212 and 127 μm thick N-115 (125 and 275 mg, respectively) while the difference in water uptake between the N-115, 180 μm thick N-117 and 254 μm thick N-1110 is smaller (275, 295 and 395 mg). Although dispersion cast (NRE-212) and extruded membranes (N-115, N-117, N-1110) can display small differences in water uptake [73], these results nevertheless suggest that water desorption is not dependent on membrane thickness but rather on the water absorbed to sulfonic acid groups as asserted by Majsztrik et al [71]. This is also evident in water desorption time where NRE-212 and N-115 desorbed within 30 minutes, while N-117 and N-1110 took approximately 50 minutes.

3.3. Liquid water imaging in Nafion membranes

To demonstrate the ability to image hydration distribution across the membranes, here the liquid water content of a partially-hydrated Nafion N-117 membrane was imaged using the proposed terahertz imaging system throughout the 120 min room temperature desorption process at 30 Hz framerate. Prior to measuring, the N-117 membrane was clamped to the sample holder and deionised water was administered directly to the lower portion of the standing membrane using a plastic squeeze bottle with a nozzle (~1 mm inner diameter). Excess water on the surface of the hydrated area, binder clips and sample holder was carefully removed using paper wipes. Figure 5 shows snapshots of the acquired terahertz images of the Nafion membrane at different timestamps of water desorption process. In order to reduce image noise and improve smoothness for qualitative water visualisation [74], median filter and contrast enhancement, via image thresholding, were applied to the terahertz images.

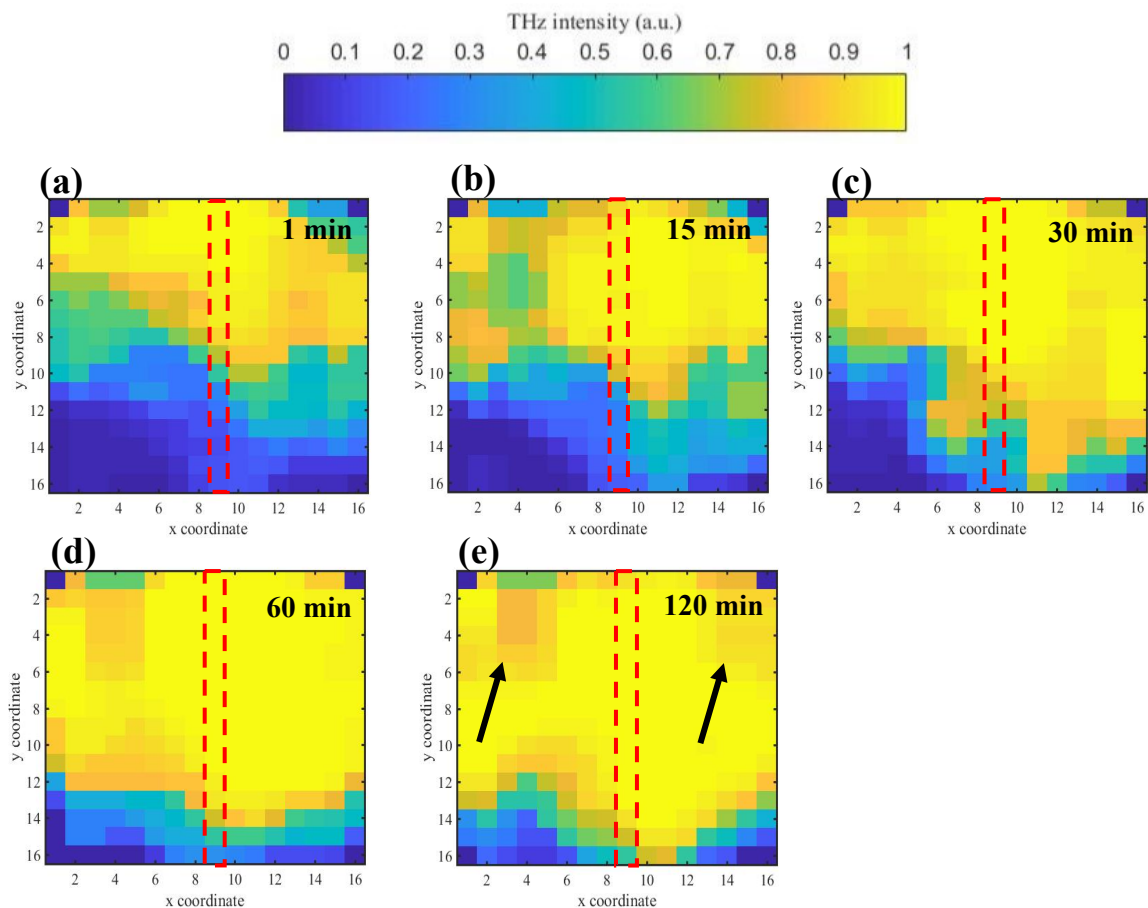


Figure 5 – Terahertz false colour images of a partially hydrated Nafion N-117 membrane during desorption process, timestamped at (a) 1min, (b) 15 min, (c) 30 min, (d) 60 min, (e) 120 min. Highlighted regions correspond to the selected pixels for further analysis in Fig. 7. Black arrows in (e) indicate ‘dimmer’ pixels related to the noise of the imaging setup.

Figure 5a displays two separate regions, ‘dry’ and ‘hydrated’ where the latter is represented by lower terahertz transmitted intensity due to beam attenuation by liquid water. Over time, as the

membrane dries, the 'hydrated' region shrinks considerably, as expected. Desorption is not uniform across the membrane area, as observed in Figure 5c, the left side of the 'hydrated' region ($x = 1$ to 8) has considerably lower terahertz transmission compared to the right side ($x = 10$ to 16) after 30 minutes of operation. In addition, two areas on the lower side of the image ($y = 12$ to 16 , $x = 1$ to 6 and $x = 13$ to 16) retains some liquid water even after 120 minutes of operation, as seen in Fig. 5e. These zones are caused by water accumulated around the binder clips used to clamp the membrane for imaging, during hydration of the lower half of the membrane. By closely examining the acquired images, various effects of noise can be observed. For example the camera provides unreliable readings at corner pixels (Figures S.1 and S.2 in Supplementary Information). Additionally, there are 'dimmer' pixels appearing randomly across the 'dry' region in Figures 5c-e. This is consistent with an independent measurement on a dry membrane where pixel intensities are also reduced around the camera edges in addition to terahertz attenuation by the Nafion membrane [75] (Figures S.3 and S.4 in Supplementary Information). A further inspection of the 'dimmer' pixels shows that intensities tend to fluctuate around 10-30% of their maximum value during the water desorption process. This is likely to be caused by the through-plane structural change that the membrane experienced: from a swollen, hydrated state (Figure 6b) to a flat and dry state (Figure 6a) due to water uptake [76]. At the same time, it should also be noted that this simple setup is also prone to vibrations from various environmental sources (Figures S.5 and S.6 in Supplementary Information) and the effect of which, can also propagate into the measurements.

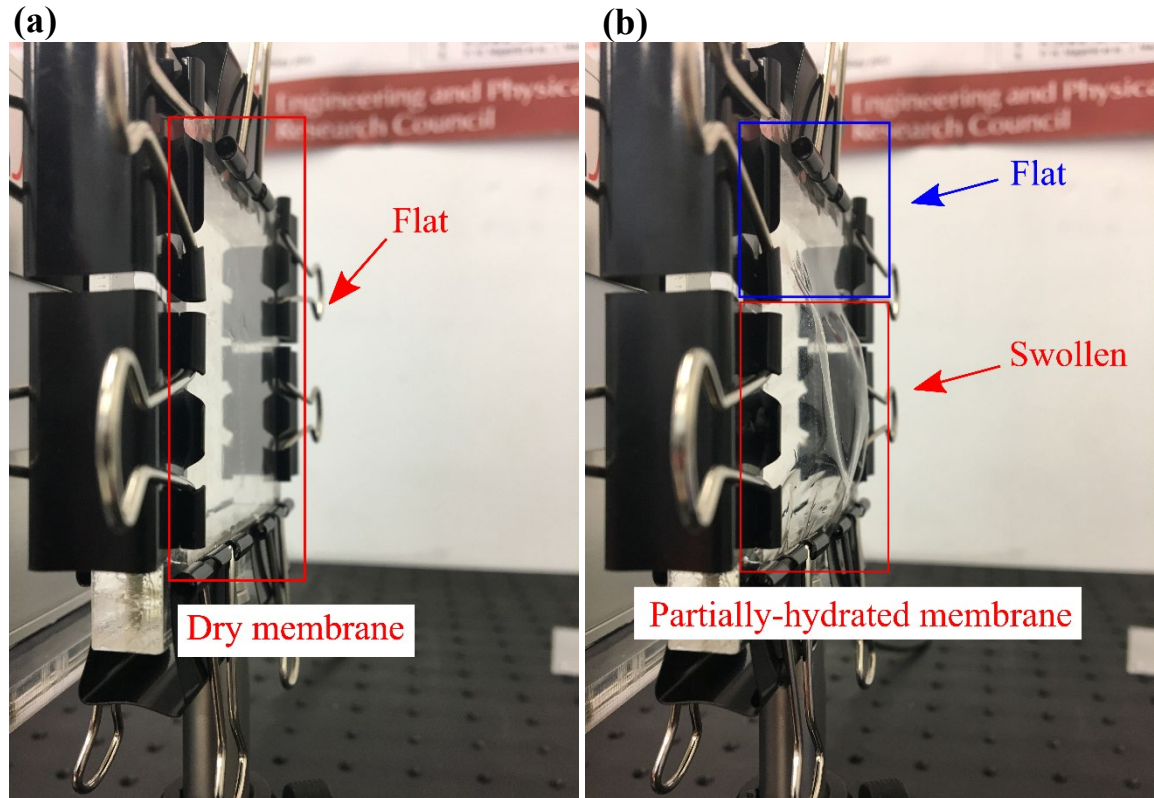


Figure 6 - Photographs of a (a) dry and (b) partially-hydrated Nafion N-117 membrane.

To further illustrate spatial differences in water content across the Nafion membrane, Figure 7 shows the pixel intensity evolution across time in the highlighted sections in Figure 5. At the beginning of the experiment, the ‘dry’ region in the upper half of the image ($y = 1$ to 8) has intensity values close to 1 (full transmission), while the ‘hydrated’ region ($y = 11$ to 16) has lower intensity values. A transition zone between the aforementioned regions ($y = 9$ to 10) bears an intermediate intensity value. Terahertz transmission on the ‘hydrated’ pixels increases gradually as the membrane approaches a dry state. Most of the ‘dry’ pixels values progressively plateau near full transmission, indicating that any small amount of water present in this region dries out relatively quickly. An exception to this trend is shown in a few pixels in the ‘dry’ region ($y = 1$ to 4) decreasing in intensity values from 1 to 15 minutes of operation. This is caused by presence of the aforementioned ‘dimmer’ pixels, observable in Figure 5b.

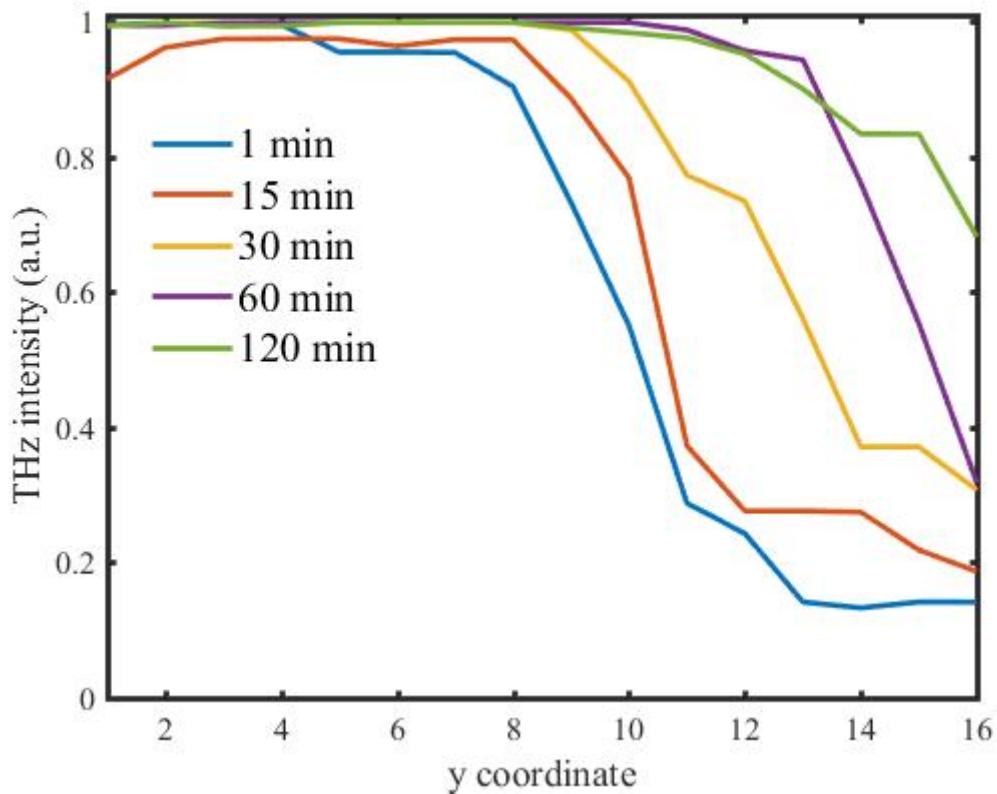


Figure 7 – Evolution of terahertz transmission in a specified pixel region along the y axis, highlighted in Figure 5.

4. Conclusion

In this study, we have investigated the feasibility of a portable, relatively inexpensive terahertz imaging system to quantify and image liquid water content across Nafion PEMs. We have demonstrated the system's sensitivity to quantify liquid water in the 25-500 μm thickness range, where the system is insensitive to thicknesses less than 25 μm . Under the assumption that membrane thickness can be taken as water thickness, we have estimated water weight loss using terahertz measurements for a desorption process while simultaneously monitoring the weight change. The outcomes are in agreement with gravimetric analysis and consistent with previously studies despite discrepancies due to residual surface water and liquid water outside the measurement window. Lastly, we demonstrated imaging liquid water spatial distribution and movement across a partially hydrated Nafion N-117 membrane during a room temperature desorption process, which is otherwise not possible with gravimetric techniques. Although the Nafion manufacturing industry for ~~commercial-high-performance~~ PEMFC applications is trending towards thinner membranes (<25~15 μm)[77,78] due to reduced proton resistance and better fuel cell performance [79], the proposed system has been demonstrated to be suitable for thicker membranes (50-254 μm), which is still relevant for PEMFC-related scientific

studies [80,81], and electrochemical applications such as PEM-electrolysis [76,82] or vanadium redox-flow batteries [83]. For thinner, state-of-the-art Nafion membranes for PEMFC, owing to the higher water sensitivity, THz-TDS is a more suitable alternative. Another advantage is the low cost nature of the terahertz imaging system, especially compared to a commercial THz-TDS system. However, better spatial resolution and water sensitivity could be achieved with more expensive micro-bolometer arrays [84]. In sum, the proposed system offers an interesting modality, and can potentially be used with vibration isolation as a non-destructive, cost-effective complementary alternative for liquid water inspection of Nafion PEM as part of future Nafion manufacturing quality control strategy.

5. Acknowledgements

The authors acknowledge the EPSRC Impact Acceleration Account EP/R511560/1. HL also acknowledges the financial support from UK Engineering and Physical Sciences Research Council Research Grant EP/R019460/1. The authors would also like to thank Dr Massimo Peruffo and Dr Jonathan Sharman, from Johnson Matthey, for fruitful discussions.

6. Appendix. Supplementary information

Supplementary data related to this article can be found online at DOI on publication.

7. References

- [1] J.C. Kurnia, A.P. Sasmito, T. Shamim, Advances in proton exchange membrane fuel cell with dead-end anode operation: A review, *Appl. Energy*. 252 (2019) 113416. doi:10.1016/j.apenergy.2019.113416.
- [2] C. Yin, Z. Wang, Y. Luo, J. Li, Y. Zhou, X. Zhang, H. Zhang, P. Fang, C. He, Thermal annealing on free volumes, crystallinity and proton conductivity of Nafion membranes, *J. Phys. Chem. Solids*. 120 (2018) 71–78. doi:10.1016/j.jpcs.2018.04.028.
- [3] J.T. Gostick, A.Z. Weber, Resistor-Network Modeling of Ionic Conduction in Polymer Electrolytes, *Electrochim. Acta*. 179 (2015) 137–145. doi:10.1016/j.electacta.2015.03.126.
- [4] Y. Cai, T. Chen, T. Yang, J. Xiao, Mechanism of water transport in serpentine cathode channels of proton exchange membrane fuel cells, *J. Power Sources*. 209 (2012) 90–104. doi:10.1016/j.jpowsour.2012.02.095.
- [5] M. Schalenbach, W. Lueke, W. Lehnert, D. Stolten, The influence of water channel geometry and proton mobility on the conductivity of Nafion®, *Electrochim. Acta*. 214 (2016) 362–369. doi:10.1016/j.electacta.2016.08.010.
- [6] W.H.J. Hogarth, J.B. Benziger, Operation of polymer electrolyte membrane fuel cells with dry feeds: Design and operating strategies, *J. Power Sources*. 159 (2006) 968–978. doi:10.1016/j.jpowsour.2005.11.079.

- [7] L. You, H. Liu, A two-phase flow and transport model for the cathode of PEM fuel cells, *Int. J. Heat Mass Transf.* 45 (2002) 2277–2287. doi:10.1016/S0017-9310(01)00322-2.
- [8] T.E. Springer, Polymer Electrolyte Fuel Cell Model, *J. Electrochem. Soc.* 138 (2006) 2334. doi:10.1149/1.2085971.
- [9] P. Pei, Y. Li, H. Xu, Z. Wu, A review on water fault diagnosis of PEMFC associated with the pressure drop, *Appl. Energy.* 173 (2016) 366–385. doi:10.1016/j.apenergy.2016.04.064.
- [10] Z. Zheng, M.C. Péra, D. Hissel, M. Becherif, K.S. Agbli, Y. Li, A double-fuzzy diagnostic methodology dedicated to online fault diagnosis of proton exchange membrane fuel cell stacks, *J. Power Sources.* 271 (2014) 570–581. doi:10.1016/j.jpowsour.2014.07.157.
- [11] J. St-Pierre, A. Wong, J. Diep, D. Kiel, Demonstration of a residence time distribution method for proton exchange membrane fuel cell evaluation, *J. Power Sources.* 164 (2007) 196–202. doi:10.1016/j.jpowsour.2006.09.103.
- [12] J. Diep, D. Kiel, J. St-Pierre, A. Wong, Development of a residence time distribution method for proton exchange membrane fuel cell evaluation, *Chem. Eng. Sci.* 62 (2006) 846–857. doi:10.1016/j.ces.2006.10.015.
- [13] S. Tsushima, K. Teranishi, S. Hirai, Magnetic Resonance Imaging of the Water Distribution within a Polymer Electrolyte Membrane in Fuel Cells, *Electrochem. Solid-State Lett.* 7 (2004) A269. doi:10.1149/1.1774971.
- [14] K.W. Feindel, S.H. Bergens, R.E. Wasylishen, The influence of membrane electrode assembly water content on the performance of a polymer electrolyte membrane fuel cell as investigated by ¹H NMR microscopy, *Phys. Chem. Chem. Phys.* 9 (2007) 1850–1857. doi:10.1039/b617551a.
- [15] S. Tsushima, K. Teranishi, K. Nishida, S. Hirai, Water content distribution in a polymer electrolyte membrane for advanced fuel cell system with liquid water supply, in: *Magn. Reson. Imaging, 2005*: pp. 255–258. doi:10.1016/j.mri.2004.11.059.
- [16] J. Bedet, G. Maranzana, S. Leclerc, O. Lottin, C. Moyne, D. Stemmelen, P. Mutzenhardt, D. Canet, Magnetic resonance imaging of water distribution and production in a 6 cm² PEMFC under operation, *Int. J. Hydrogen Energy.* 33 (2008) 3146–3149. doi:10.1016/j.ijhydene.2008.01.053.
- [17] K.R. Minard, V. V. Viswanathan, P.D. Majors, L.Q. Wang, P.C. Rieke, Magnetic resonance imaging (MRI) of PEM dehydration and gas manifold flooding during continuous fuel cell operation, *J. Power Sources.* 161 (2006) 856–863. doi:10.1016/j.jpowsour.2006.04.125.
- [18] J.M. Lamanna, S. Chakraborty, J.J. Gagliardo, M.M. Mench, Isolation of transport mechanisms in PEFCs using high resolution neutron imaging, *Int. J. Hydrogen Energy.* 39 (2014) 3387–3396. doi:10.1016/j.ijhydene.2013.12.021.
- [19] S.S. Alrwashdeh, I. Manke, H. Markötter, J. Haußmann, N. Kardjilov, A. Hilger, M.J. Kermani, M. Klages, A.M. Al-Falahat, J. Scholta, J. Banhart, Neutron radiographic in operando investigation of water transport in polymer electrolyte membrane fuel cells with channel barriers, *Energy Convers. Manag.* 148 (2017) 604–610.

doi:10.1016/j.enconman.2017.06.032.

- [20] A. Turhan, S. Kim, M. Hatzell, M.M. Mench, Impact of channel wall hydrophobicity on through-plane water distribution and flooding behavior in a polymer electrolyte fuel cell, *Electrochim. Acta.* 55 (2010) 2734–2745. doi:10.1016/j.electacta.2009.11.095.
- [21] M.A. Hickner, N.P. Siegel, K.S. Chen, D.S. Hussey, D.L. Jacobson, Observations of Transient Flooding in a Proton Exchange Membrane Fuel Cell Using Time-Resolved Neutron Radiography, *J. Electrochem. Soc.* 157 (2009) B32. doi:10.1149/1.3250864.
- [22] A. Iranzo, P. Boillat, J. Biesdorf, A. Salva, Investigation of the liquid water distributions in a 50cm² PEM fuel cell: Effects of reactants relative humidity, current density, and cathode stoichiometry, *Energy.* 82 (2015) 914–921. doi:10.1016/j.energy.2015.01.101.
- [23] A. Iranzo, A. Salva, P. Boillat, J. Biesdorf, E. Tapia, F. Rosa, Water build-up and evolution during the start-up of a PEMFC: Visualization by means of Neutron Imaging, *Int. J. Hydrogen Energy.* 42 (2017) 13839–13849. doi:10.1016/j.ijhydene.2016.11.076.
- [24] I. Manke, C. Hartnig, M. Grünerbel, W. Lehnert, N. Kardjilov, A. Haibel, A. Hilger, J. Banhart, H. Rieseemeier, Investigation of water evolution and transport in fuel cells with high resolution synchrotron x-ray radiography, *Appl. Phys. Lett.* 90 (2007). doi:10.1063/1.2731440.
- [25] C. Hartnig, I. Manke, R. Kuhn, S. Kleinau, J. Goebbels, J. Banhart, High-resolution in-plane investigation of the water evolution and transport in PEM fuel cells, *J. Power Sources.* 188 (2009) 468–474. doi:10.1016/j.jpowsour.2008.12.023.
- [26] P. Krüger, H. Markötter, J. Haußmann, M. Klages, T. Arlt, J. Banhart, C. Hartnig, I. Manke, J. Scholta, Synchrotron X-ray tomography for investigations of water distribution in polymer electrolyte membrane fuel cells, *J. Power Sources.* 196 (2011) 5250–5255. doi:10.1016/j.jpowsour.2010.09.042.
- [27] T. Mukaide, S. Mogi, J. Yamamoto, A. Morita, S. Koji, K. Takada, K. Uesugi, K. Kajiwara, T. Noma, In situ observation of water distribution and behaviour in a polymer electrolyte fuel cell by synchrotron X-ray imaging, *J. Synchrotron Radiat.* 15 (2008) 329–334. doi:10.1107/S0909049508006638.
- [28] S.J. Lee, S.G. Kim, G.G. Park, C.S. Kim, Quantitative visualization of temporal water evolution in an operating polymer electrolyte fuel cell, *Int. J. Hydrogen Energy.* 35 (2010) 10457–10463. doi:10.1016/j.ijhydene.2010.07.173.
- [29] J. Lee, R. Yip, P. Antonacci, N. Ge, T. Kotaka, Y. Tabuchi, A. Bazylak, Synchrotron Investigation of Microporous Layer Thickness on Liquid Water Distribution in a PEM Fuel Cell, *J. Electrochem. Soc.* 162 (2015) F669–F676. doi:10.1149/2.0221507jes.
- [30] M.M. Daino, Z. Lu, J.M. LaManna, J.P. Owejan, T.A. Trabold, S.G. Kandlikar, Through-Plane Water Transport Visualization in a PEMFC by Visible and Infrared Imaging, *Electrochem. Solid-State Lett.* 14 (2011) B51. doi:10.1149/1.3560163.
- [31] K. Fushinobu, K. Shimizu, N. Miki, K. Okazaki, Optical Measurement Technique of Water Contents in Polymer Membrane for PEFCs, *J. Fuel Cell Sci. Technol.* 3 (2006) 13. doi:10.1115/1.2133801.
- [32] R.M. Aslam, D.B. Ingham, M.S. Ismail, K.J. Hughes, L. Ma, M. Pourkashanian,

- Simultaneous direct visualisation of liquid water in the cathode and anode serpentine flow channels of proton exchange membrane (PEM) fuel cells, *J. Energy Inst.* 91 (2018) 1057–1070. doi:10.1016/j.joei.2017.07.003.
- [33] M. Rahimi-Esbo, A. Ramiar, A.A. Ranjbar, E. Alizadeh, Design, manufacturing, assembling and testing of a transparent PEM fuel cell for investigation of water management and contact resistance at dead-end mode, *Int. J. Hydrogen Energy.* 42 (2017) 11673–11688. doi:10.1016/j.ijhydene.2017.02.030.
- [34] M. Yamauchi, K. Sugiura, T. Yamauchi, T. Taniguchi, Y. Itoh, Proposal for an optimum water management method using two-pole simultaneous measurement, *J. Power Sources.* 193 (2009) 1–8. doi:10.1016/j.jpowsour.2009.02.078.
- [35] I.S. Hussaini, C.Y. Wang, Visualization and quantification of cathode channel flooding in PEM fuel cells, *J. Power Sources.* 187 (2009) 444–451. doi:10.1016/j.jpowsour.2008.11.030.
- [36] T. Ous, C. Arcoumanis, Visualisation of water droplets during the operation of PEM fuel cells, *J. Power Sources.* 173 (2007) 137–148. doi:10.1016/j.jpowsour.2007.04.075.
- [37] X.G. Yang, F.Y. Zhang, A.L. Lubawy, C.Y. Wang, Visualization of Liquid Water Transport in a PEFC, *Electrochem. Solid-State Lett.* 7 (2004) A408. doi:10.1149/1.1803051.
- [38] A. Bazylak, D. Sinton, Z.S. Liu, N. Djilali, Effect of compression on liquid water transport and microstructure of PEMFC gas diffusion layers, *J. Power Sources.* 163 (2007) 784–792. doi:10.1016/j.jpowsour.2006.09.045.
- [39] S. Litster, D. Sinton, N. Djilali, Ex situ visualization of liquid water transport in PEM fuel cell gas diffusion layers, *J. Power Sources.* 154 (2006) 95–105. doi:10.1016/j.jpowsour.2005.03.199.
- [40] A. Bazylak, Liquid water visualization in PEM fuel cells: A review, *Int. J. Hydrogen Energy.* 34 (2009) 3845–3857. doi:10.1016/j.ijhydene.2009.02.084.
- [41] S. Tsushima, S. Hirai, In situ diagnostics for water transport in proton exchange membrane fuel cells, *Prog. Energy Combust. Sci.* 37 (2011) 204–220. doi:10.1016/j.pecs.2010.06.001.
- [42] J. St-Pierre, PEMFC In Situ Liquid-Water-Content Monitoring Status, *J. Electrochem. Soc.* 154 (2007) B724. doi:10.1149/1.2737542.
- [43] M.M. Daino, S.G. Kandlikar, Evaluation of Imaging Techniques Applied to Water Management Research in PEMFCs, *Proc. 7th Int. Conf. Nanochannels, Microchannels, Minichannels 2009, ICNMM2009.* (2010) 467–479. doi:10.1115/icnmm2009-82031.
- [44] I. Manke, C. Hartnig, M. Grünerbel, W. Lehnert, N. Kardjilov, A. Haibel, A. Hilger, J. Banhart, H. Riesemeier, Investigation of water evolution and transport in fuel cells with high resolution synchrotron x-ray radiography, *Appl. Phys. Lett.* 90 (2007). doi:10.1063/1.2731440.
- [45] B. Mecheri, V. Felice, Z. Zhang, A. D'Epifanio, S. Licoccia, A.C. Tavares, DSC and DVS investigation of water mobility in Nafion/zeolite composite membranes for fuel cell applications, *J. Phys. Chem. C.* (2012). doi:10.1021/jp301762h.

- [46] F.M. Collette, C. Lorentz, G. Gebel, F. Thominet, Hygrothermal aging of Nafion®, *J. Memb. Sci.* (2009). doi:10.1016/j.memsci.2008.11.048.
- [47] B. Legros, P.-X. Thivel, Y. Bultel, M. Boinet, R.P. Nogueira, Electrochemical Impedance and Acoustic Emission Survey of Water Desorption in Nafion Membranes, *Electrochem. Solid-State Lett.* 12 (2009) B116. doi:10.1149/1.3131728.
- [48] Y. Tabuchi, R. Ito, S. Tsushima, S. Hirai, Analysis of in situ water transport in Nafion® by confocal micro-Raman spectroscopy, *J. Power Sources.* (2011). doi:10.1016/j.jpowsour.2010.07.078.
- [49] S. Deabate, R. Fatnassi, P. Sizat, P. Huguet, In situ confocal-Raman measurement of water and methanol concentration profiles in Nafion® membrane under cross-transport conditions, *J. Power Sources.* (2008). doi:10.1016/j.jpowsour.2007.10.044.
- [50] M.S. Mu'min, T. Böhm, R. Moroni, R. Zengerle, S. Thiele, S. Vierrath, M. Breitwieser, Local hydration in ionomer composite membranes determined with confocal Raman microscopy, *J. Memb. Sci.* (2019). doi:10.1016/j.memsci.2019.05.032.
- [51] P. Huguet, A. Morin, G. Gebel, S. Deabate, A.K. Sutor, Z. Peng, In situ analysis of water management in operating fuel cells by confocal Raman spectroscopy, *Electrochem. Commun.* (2011). doi:10.1016/j.elecom.2011.02.008.
- [52] S. Yassin, K. Su, H. Lin, L.F. Gladden, J.A. Zeitler, Diffusion and swelling measurements in pharmaceutical powder compacts using terahertz pulsed imaging, *J. Pharm. Sci.* 104 (2015) 1658–1667. doi:10.1002/jps.24376.
- [53] H. Lin, Y. Dong, Y. Shen, J.A. Zeitler, Quantifying Pharmaceutical Film Coating with Optical Coherence Tomography and Terahertz Pulsed Imaging: An Evaluation, *J. Pharm. Sci.* 104 (2015) 3377–3385. doi:10.1002/jps.24535.
- [54] H. Lin, Y. Dong, D. Markl, B.M. Williams, Y. Zheng, Y. Shen, J.A. Zeitler, Measurement of the Intertablet Coating Uniformity of a Pharmaceutical Pan Coating Process With Combined Terahertz and Optical Coherence Tomography In-Line Sensing, *J. Pharm. Sci.* 106 (2017) 1075–1084. doi:10.1016/j.xphs.2016.12.012.
- [55] H. Lin, R.K. May, M.J. Evans, S. Zhong, L.F. Gladden, Y. Shen, J.A. Zeitler, Impact of Processing Conditions on Inter-tablet Coating Thickness Variations Measured by Terahertz In-Line Sensing, *J. Pharm. Sci.* 104 (2015) 2513–2522. doi:10.1002/jps.24503.
- [56] G. Ok, H.J. Kim, H.S. Chun, S.W. Choi, Foreign-body detection in dry food using continuous sub-terahertz wave imaging, *Food Control.* 42 (2014) 284–289. doi:10.1016/j.foodcont.2014.02.021.
- [57] Y. Oyama, L. Zhen, T. Tanabe, M. Kagaya, Sub-terahertz imaging of defects in building blocks, *NDT E Int.* 42 (2009) 28–33. doi:10.1016/j.ndteint.2008.08.002.
- [58] P. Thamboon, P. Buaphad, C. Thongbai, J. Saisud, K. Kusoljariyakul, M.W. Rhodes, T. Vilaithong, Investigation of water distribution in proton exchange membrane fuel cells via Terahertz imaging, *Nucl. Instruments Methods Phys. Res. Sect. A Accel. Spectrometers, Detect. Assoc. Equip.* 637 (2011) S161–S164. doi:10.1016/j.nima.2010.02.047.
- [59] P. Buaphad, P. Thamboon, N. Kangrang, M.W. Rhodes, C. Thongbai, Femtoelectron-

- Based Terahertz Imaging of Hydration State in a Proton Exchange Membrane Fuel Cell, *J. Infrared, Millimeter, Terahertz Waves*. 36 (2015) 745–755. doi:10.1007/s10762-015-0166-4.
- [60] S. Ray, N. Devi, J. Dash, G. Rambabu, S.D. Bhat, B. Pesala, Enhancement of water retention in UV-exposed fuel-cell proton exchange membranes studied using terahertz spectroscopy, *Terahertz, RF, Millimeter, Submillimeter-Wave Technol. Appl.* IX. 9747 (2016) 97470P. doi:10.1117/12.2212388.
- [61] N. Devi, S. Ray, A. Shukla, S.D. Bhat, B. Pesala, Tracking the hydration dynamics of Nafion fuel cell membranes using terahertz spectroscopy, in: 2019: p. 64. doi:10.1117/12.2511029.
- [62] H. Kita, K. Okamoto, S. Mukai, Dielectric properties of polymers containing dispersed TCNQ salts, *J. Appl. Polym. Sci.* 31 (1986) 1383–1392. doi:10.1002/app.1986.070310522.
- [63] Q. Duan, H. Wang, J. Benziger, Transport of liquid water through Nafion membranes, *J. Memb. Sci.* 392–393 (2012) 88–94. doi:10.1016/j.memsci.2011.12.004.
- [64] J.T. Hinatsu, Water Uptake of Perfluorosulfonic Acid Membranes from Liquid Water and Water Vapor, *J. Electrochem. Soc.* 141 (2006) 1493. doi:10.1149/1.2054951.
- [65] C.B. Reid, E. Pickwell-Macpherson, J.G. Laufer, A.P. Gibson, J.C. Hebden, V.P. Wallace, Accuracy and resolution of THz reflection spectroscopy for medical imaging, *Phys. Med. Biol.* 55 (2010) 4825–4838. doi:10.1088/0031-9155/55/16/013.
- [66] J. Xu, K.W. Plaxco, S.J. Allen, Absorption spectra of liquid water and aqueous buffers between 0.3 and 3. 72 THz, *J. Chem. Phys.* 124 (2006). doi:10.1063/1.2151267.
- [67] J.T. Kindt, C.A. Schmuttenmaer, Far-Infrared Dielectric Properties of Polar Liquids Probed by Femtosecond Terahertz Pulse Spectroscopy †, *J. Phys. Chem.* 100 (2002) 10373–10379. doi:10.1021/jp960141g.
- [68] L. Thrane, R.H. Jacobsen, P. Uhd Jepsen, S.R. Keiding, THz reflection spectroscopy of liquid water, *Chem. Phys. Lett.* 240 (1995) 330–333. doi:10.1016/0009-2614(95)00543-D.
- [69] J.E. Bertie, Z. Lan, Infrared intensities of liquids XX: The intensity of the OH stretching band of liquid water revisited, and the best current values of the optical constants of H₂O(l) at 25 °C between 15,000 and 1 cm⁻¹, *Appl. Spectrosc.* 50 (1996) 1047–1057. doi:10.1366/0003702963905385.
- [70] K. Schmidt-Rohr, Q. Chen, Parallel cylindrical water nanochannels in Nafion fuel-cell membranes, *Nat. Mater.* 7 (2008) 75–83. doi:10.1038/nmat2074.
- [71] P.W. Majsztrik, M.B. Satterfield, A.B. Bocarsly, J.B. Benziger, Water sorption, desorption and transport in Nafion membranes, *J. Memb. Sci.* 301 (2007) 93–106. doi:10.1016/j.memsci.2007.06.022.
- [72] M.B. Satterfield, J.B. Benziger, Non-Fickian water vapor sorption dynamics by nafion membranes, *J. Phys. Chem. B.* 112 (2008) 3693–3704. doi:10.1021/jp7103243.
- [73] J. Peron, A. Mani, X. Zhao, D. Edwards, M. Adachi, T. Soboleva, Z. Shi, Z. Xie, T. Navessin, S. Holdcroft, Properties of Nafion® NR-211 membranes for PEMFCs, *J. Memb. Sci.* 356 (2010) 44–51. doi:10.1016/j.memsci.2010.03.025.

- [74] H. Zhang, S. Sfarra, K. Saluja, J. Peeters, J. Fleuret, Y. Duan, H. Fernandes, N. Avdelidis, C. Ibarra-Castanedo, X. Maldague, Non-destructive Investigation of Paintings on Canvas by Continuous Wave Terahertz Imaging and Flash Thermography, *J. Nondestruct. Eval.* 36 (2017). doi:10.1007/s10921-017-0414-8.
- [75] S.O. Yurchenko, K.I. Zaytsev, Spectroscopy of nafion in terahertz frequency range, *J. Appl. Phys.* 116 (2014). doi:10.1063/1.4896194.
- [76] H. Ito, T. Maeda, A. Nakano, H. Takenaka, Properties of Nafion membranes under PEM water electrolysis conditions, *Int. J. Hydrog. Energy.* 36 (2011) 10527–10540. doi:10.1016/j.ijhydene.2011.05.127.
- [77] A. Orfanidi, P. Madkikar, H.A. El-Sayed, G.S. Harzer, T. Kratky, H.A. Gasteiger, The key to high performance low pt loaded electrodes, *J. Electrochem. Soc.* (2017). doi:10.1149/2.1621704jes.
- [78] V. Yarlagadda, M.K. Carpenter, T.E. Moylan, R.S. Kukreja, R. Koestner, W. Gu, L. Thompson, A. Kongkanand, Boosting Fuel Cell Performance with Accessible Carbon Mesopores, *ACS Energy Lett.* (2018). doi:10.1021/acseenergylett.8b00186.
- [79] A. Kusoglu, A.Z. Weber, New Insights into Perfluorinated Sulfonic-Acid Ionomers, *Chem. Rev.* (2017). doi:10.1021/acs.chemrev.6b00159.
- [80] D. Cha, S.W. Jeon, W. Yang, D. Kim, Y. Kim, Comparative performance evaluation of self-humidifying PEMFCs with short-side-chain and long-side-chain membranes under various operating conditions, *Energy.* 150 (2018) 320–328. doi:10.1016/j.energy.2018.02.133.
- [81] F. Trombetta, D.W. Lima, F. Fiegenbaum, M.R. Becker, M.O. de Souza, E.M.A. Martini, C 16 MI.OTf ionic liquid on Pt/C and PtMo/C anodes improves the PEMFC performance, *Int. J. Hydrogen Energy.* 43 (2018) 6945–6953. doi:10.1016/j.ijhydene.2018.02.104.
- [82] L.A. King, M.A. Hubert, C. Capuano, J. Manco, N. Danilovic, E. Valle, T.R. Hellstern, K. Ayers, T.F. Jaramillo, Non-precious metal hydrogen catalyst in commercial polymer electrolyte membrane electrolyzers, *Nat. Nanotechnol.* Accepted (2019). doi:10.1038/s41565-019-0550-7.
- [83] Y. Lee, S. Kim, R. Hempelmann, J.H. Jang, H.J. Kim, J. Han, J. Kim, D. Henkensmeier, Nafion membranes with a sulfonated organic additive for the use in vanadium redox flow batteries, *J. Appl. Polym. Sci.* 136 (2019) 8–13. doi:10.1002/app.47547.
- [84] N. Oda, S. Kurashina, M. Miyoshi, K. Doi, T. Ishi, T. Sudou, T. Morimoto, H. Goto, T. Sasaki, Microbolometer Terahertz Focal Plane Array and Camera with Improved Sensitivity in the Sub-Terahertz Region, *J. Infrared, Millimeter, Terahertz Waves.* (2015). doi:10.1007/s10762-015-0184-2.

Figure captions

Figure 1 – (a) Schematic of the terahertz imaging system for simultaneous gravimetric analysis (b) Front view of the sample holder featuring Nafion sample, binder clips, and area used for terahertz measurements.

Figure 2 – Terahertz false colour images of the (a) ‘dry’ and (b) ‘hydrated’ liquid cell of spacer thickness 50 μm . Highlighted region corresponds to the aperture in the liquid cell and is used for quantification purposes.

Figure 3 – Water quantitative analysis showing the measured relative transmitted terahertz intensities at a 25-500 μm range of liquid water thicknesses, against the expected values using Beer Lambert Law with absorption coefficients of 9-13 mm^{-1} at 100 GHz at 25°C, with maximum (13 mm^{-1}) and minimum (9 mm^{-1}) values displayed at the boundaries of shaded area. The vertical error bars refer to standard deviation between 5 experiments. The horizontal error bars refer to thickness tolerances of the spacer material.

Figure 4 – Water desorption from saturated Nafion (a) NRE-212, (b) N-115, (c) N-117 and (d) N-1110. Blue and red line and shade represent the mean and standard deviation of estimated liquid water weight from terahertz intensities and actual measured liquid water weight from gravimetric analysis, respectively, from 4 repeated experiments. For clarity, a reduced scale inset is present on (a).

Figure 5 – Terahertz false colour images of a partially hydrated Nafion N-117 membrane during desorption process, timestamped at (a) 1min, (b) 15 min, (c) 30 min, (d) 60 min, (e) 120 min. Highlighted regions correspond to the selected pixels for further analysis in Fig. 7. Black arrows in (e) indicate ‘dimmer’ pixels related to the noise of the imaging setup.

Figure 6 - Photographs of a (a) dry and (b) partially-hydrated Nafion N-117 membrane.

Figure 7 – Evolution of terahertz transmission in a specified pixel region along the y axis, highlighted in Figure 5.